FE ANALYSIS OF INTEGRITY OF DISSIMILAR WELD JOINTS OF MODIFIED 9Cr-1Mo STEEL UNDER CREEP CONDITION

Sunil Goyal, K. Laha, K. S. Chandravathi, J. Ganesh Kumar, P. Parameswaran and M. D. Mathew
Metallurgy and Materials Group, Indira Gandhi Centre for Atomic Research, Kalpakkam – 603 102, INDIA
E-mail of corresponding author: goyal@igcar.gov.in

ABSTRACT

Integrity of Modified 9Cr-1Mo steel / Alloy 800 dissimilar joint under creep conditions has been assessed based on the detailed analysis of stress distribution across the heterogeneous microstructure of the joint by finite element (FE) analysis. The dissimilar weld joint was fabricated by shielded metal arc welding process employing Inconel 182 electrode. Creep tests at 823 K over a stress range of 100- 380 MPa were carried out on the steel base metal and dissimilar weld joint. The joint displayed lower creep rupture strength than its ferritic base metal. Failure in the dissimilar joint occurred at the ferritic / austenitic weld interface. Cavity nucleation associated with weld interface particles led to the premature failure of the dissimilar joint. Finite element analysis of stress distribution across the weld joint was carried out considering the micro-mechanical strength inhomogeneity across it. The estimated higher von-Mises stress and higher principal stress near surface region of weld interface of the joint induced preferential creep cavitation at ferritic /austenitic weld interface. Role of precipitate in enhancing creep cavitation at the weld interface of the joint has been elucidated based on the FE analysis of stress distribution across it.

INTRODUCTION

Dissimilar weld joints between Cr-Mo ferritic steels and austenitic stainless steels are used extensively in conventional as well as in nuclear power generating plants and petrochemical industries. In the steam generator circuit of sodium cooled fast breeder reactors (SFRs), 316L(N) austenitic stainless steel pipes from the intermediate heat exchangers are required to join with the Modified 9Cr-1Mo ferritic steel pipes of steam generators. In such a joint, a ferritic / austenitic transition bond is formed across which the chemical composition, microstructure, stress state, physical properties such as thermal expansion coefficient and thermal conductivity, and mechanical properties vary quite appreciably. The mismatch in thermal expansion coefficient across the joint is reduced with the insertion of an Alloy 800 piece and adopting Inconel 182 welding electrode having thermal expansion coefficients intermediate between austenitic and ferritic steels [1]. However, premature creep failure is encountered in such dissimilar weld joint [2-7]. An understanding of the microstructural changes across the weld bond between ferritic and austenitic alloys and their effects on high temperature creep deformation and fracture behaviour are of primary concern for a realistic life prediction of the dissimilar weld joints [8-14]. Further, the combination of material, loading conditions and geometry and size of the weld joint can lead to the presence of complex stress state and to local constraint that are found to be of great influence is causing reduction in creep life of dissimilar weld joints [15-17].

In the dissimilar weld joints, each distinct microstructural region is surrounded by regions that have different creep flow behaviors. The consequence is that the flow of the high creep resistant region is enhanced by the surrounding regions having lower creep resistance. The constraint effect leads to stress redistribution and development of multiaxial state of stress [18,19] across the weld joint, which influence the creep cavity nucleation and their growth across the weld joint. The assessment of weld joint performance under creep conditions depends on how the microstructure varies across it, in particular the extent, geometry, distribution and property differences, affect the localized creep deformation and cavitation behaviour leading to failure. Attempts have been made to estimate stress and strain distributions developed across the weld joints and its consequences on creep cavitation [20-22] using FE analysis.

This study aims to understand the creep rupture behaviour of the Mod. 9Cr-1Mo / Alloy 800 dissimilar joints welded with Inconel 182 electrode. Detailed microstructural, micro-hardness, elemental distribution and FE analysis of stress state studies across the weld interface are carried out. The role of precipitates at ferritic / austenitic interface in enhancing the creep cavitation has been illustrated based on the stress distributions across it by FE analysis.

EXPERIMENTAL

Materials and Creep Testing

Dissimilar weld joint of the Mod. 9Cr-1Mo ferritic steel with Alloy 800 was fabricated by the shielded metal arc welding (SMAW) process using Inconel 182 electrodes. Chemical compositions of the base metals and the deposited weld metal are shown in Table 1. The weld pad was subjected to post weld heat treatment (PWHT) at 1033 K for one hour, and were subsequently X-ray radiographed for its soundness. Optical and scanning electron microcopy (SEM) metallographic examination and micro-hardness testing of the weld joints were carried out in the as-welded, post weld heat treated and creep tested conditions. A two-stage etching procedure was used to reveal the microstructures of the different zones of dissimilar weld joint. An electrolytic etching in 10% chromic acid with 6 V was carried out to reveal the microstructures of the weld interface, Inconel weld metal and Alloy 800 base metal; whereas an immersion etching in Villela's reagent was found to etch the ferritic part of the joints adequately. Creep rupture tests were performed on the ferritic steel base metal and on the dissimilar weld joint at 823 K over a stress range 100 - 380 MPa. Temperature was controlled within ± 2 K during the creep test along the gauge length of creep specimen.

Table 1 Chemical composition (wt. %) of the material used

Materials/ elements	C	Si	Mn	P	S	Cr	Mo	Ni	Al	Co	Nb	V	N	Ti	Fe
Mod. 9Cr-1Mo	0.096	0.32	0.46	0.01	0.008	8.72	0.90	0.10	-	-	0.08	0.22	0.05		
Alloy 800	0.03	0.27	0.86	0.009	0.009	19.5	0.10	30.8	0.14	0.2	0.017	-	-	0.39	bal
Inconel 182	0.05	0.56	7.84	0.01	0.004	13.8	-	66.2	-	-	1.84	-	-	0.40	bal

Finite Element Analysis

The variation of microstructures from wrought base metal through transformed heat affected zones (HAZ) to cast base metal in weld joint, gives rise to considerable inhomogeneity with respect to mechanical strength and ductility across it. The multiaxial state of stress across it during creep exposure arises due to the strength inhomogeneity have been analyzed by 2D axisymmetric FE analysis. Norton's creep law relating the steady state creep rate with applied stress ($\dot{\varepsilon}_s = A\sigma^n$, where $\dot{\varepsilon}_s$ is the strain rate (h^{-1}), σ is the stress (MPa) and A and n are constants) was used as a constitutive equation for the analysis. In order to incorporate the material model in FE analysis, creep tests on the different constituents of joints viz. ferritic base metal, Inconel weld metal and HAZ comprising coarse prior austenitic grain HAZ (CGHAZ), fine prior austenitic grain HAZ (FGHAZ), and intercritical region of HAZ (ICHAZ) in ferritic steels and weld interface zone were carried out at 823 K over a stress range 100-380 MPa. The different microstructures in the HAZ of the weld joint were simulated on the base metal by isothermal heat treatment cycles because of the practical difficulty in extracting specimens for creep tests from small extent of HAZ. The simulation was based on the detailed comparison of the microstructures, prior-austenitic grain size and the hardness of the heat-treated samples with those of in the HAZ of actual weld joint. The mixed weld interface zone was simulated by depositing Mod 9Cr-1Mo and Inconel 182 electrodes simultaneously in a weld groove. Widths of the different microstructural zones in the weld joint were identified from the hardness profile and microstructural variation across the joint and these were used to model the geometry of the joint in FE analysis. The finite element simulations were carried out using ABAQUS 6.9 FE software. Specimen was modeled using 4 noded quadrilateral elements with appropriate boundary conditions as shown in Fig. 1(a). Weld joint specimen had a gauge length of 50 mm but only one fourth of the specimen was modeled for the analysis because of geometrical symmetry and also due the creep failure of the joint in the ferritic side of the weld interface. The weld angle was considered as 0 degree for the analysis. The regions of high stress gradient were refined to obtain more accurate stress and strain distributions across the weld joints specimen without sacrificing the computational time. Automatic time increment was controlled by accuracy tolerance defined by stress error acceptable divided by elastic modulus. A mesh convergence analysis was first performed to avoid the effect of mesh size. This was carried out by running different models with varying element size until the difference in results between two consecutive models was negligible. Young's modulus and Poison's ratio of the different constituents of the ferritic steel weld joint were chosen as 160 GPa and 0.3 respectively. Young's modulus and Poison's ratio of the weld metal and ferritic / austenitic weld interface were chosen as 185 GPa and 0.3 respectively. The analysis was carried out for creep test at 823 K and 160 MPa and was continued until the stationary state of stress distribution reached. It was observed that the stress distribution in FE analysis saturated after 7,000 hours of creep exposure; whereas under similar conditions actual weld joints specimen failed in 10,547 hours. In order to study the effect of precipitate on creep cavitation, FE analysis of stress distribution across it was carried out. The model consisted of 3D 8 noded brick elements for both

the matrix and precipitate as shown in Fig. 1(b). Precipitate size was considered as 0.2 μm, typically observed in the HAZ of Cr-Mo steel weld joints. The model assumed a spherical precipitate of radius 0.2 μm embedded in a matrix of 4×4×4 μm. The typical distance between two precipitates was assumed to be 4 μm. The 3D model used in the current study was 1/8 of the physical model. The elastic modulus and Poisson's ratio of the precipitate ($Cr_{23}C_6$) were taken as 218 GPa and 0.367 respectively. The matrix was considered to deform both elastically and inelastically whereas precipitate was considered to deform elastically because of its very high hardness.

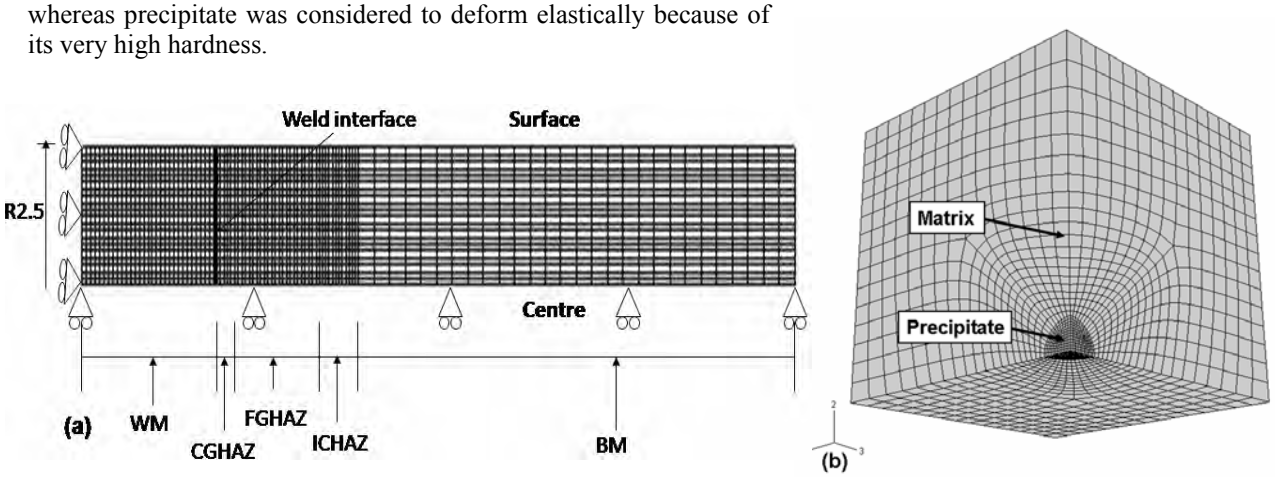

Fig. 1: (a) - Typical FE mesh for weld joint specimen used in the analysis and (b) - Typical FE mesh used to analyze the stress distribution across the precipitate.

RESULTS AND DISCUSSIONS

Creep Rupture Behaviour and Failure Location

Microstructure across the dissimilar weld joints was found to vary considerably. It consisted of ferritic Cr-Mo base metal, austenitic Alloy 800 base metal and Inconel weld metal, HAZs in both the ferritic and austenitic base metals and distinct interface (Fig. 2) across the ferritic base metal and austenitic weld metal. Mixing of Mod. 9Cr-1Mo base metal and Inconel 182 welding electrode resulted in distinct interface structure (Fig. 2(a)) with a series of precipitate particles towards the ferritic side of the interface (Fig. 2(b)). Hardness change across the weld interfaces of dissimilar weld joint (Fig. 3) reflects the microstructural variation across the joint. Variations of creep rupture life with applied stress at 823 K for the ferritic steel base metal and its dissimilar weld joint are shown in Fig. 4. The dissimilar weld joint of the ferritic steel had lower creep rupture strength than that of the ferritic steel base metal. The stress rupture life variation of the dissimilar weld joint showed a two-slope behaviour.

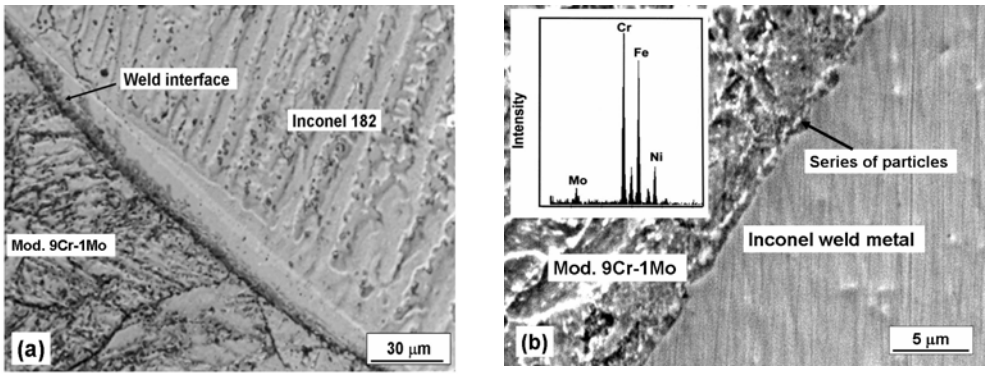

Fig. 2: Optical microstructure across the 9Cr-1Mo dissimilar weld joint, showing; (a) partial conversion of light-etched band into dark-etched band on PWHT; and SEM micrographs across weld interface, showing formation of series of precipitate in ferritic steel at a distance less than 1 μm from the interface of (b) 9Cr-1Mo weld joint.

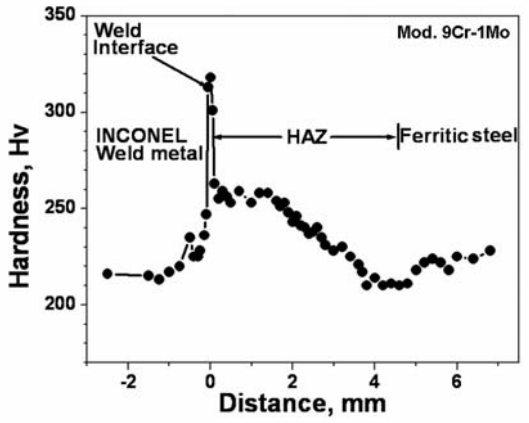

Fig. 3

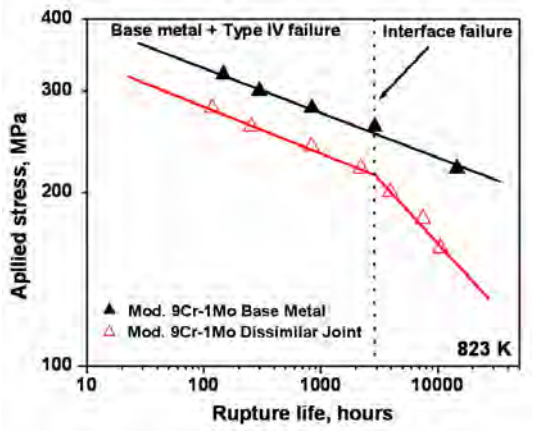

Fig. 4

Fig. 3: Hardness variation across the Inconel 182/ferritic steel weld joint interface.
Fig. 4: Creep rupture lives of dissimilar weld joint with base metal.

The fracture mode and the location of creep failure in the dissimilar weld joint were found to vary with the applied stress (Fig. 5). At relatively higher applied stresses, the failure in the dissimilar weld joint occurred in the ferritic steel base metal away from the weld zone (Fig. 5(a)). At lower applied stresses, the failure in the dissimilar weld joint occurred at the weld interface between the ferritic steel and Inconel weld metal (Fig. 5(b)) and was associated with very low creep ductility.

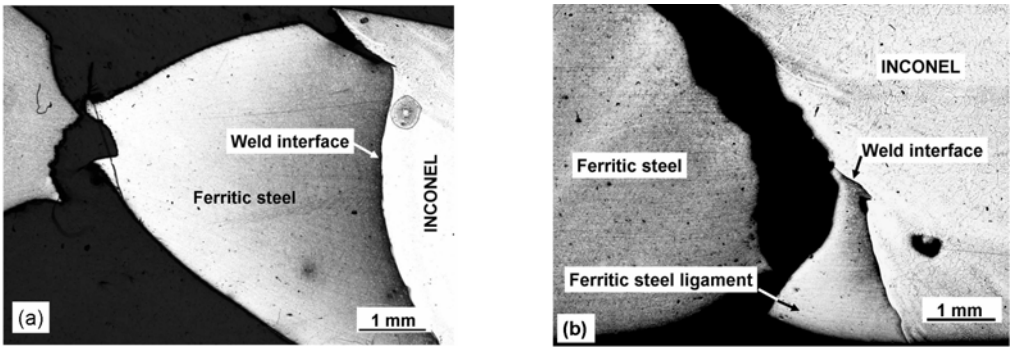

Fig. 5: Creep failure locations in the weld joint; (a) Ferritic steel base metal (260 MPa, 823 K, t_r = 256 h) and (b) Interface (with ferrite ligament) and ferritic/austenitic weld interface(160 MPa, 823 K, t_r = 10547 h).

The interface cracking coincided with the change in slope in the variation of rupture life with applied stress (Fig. 4), similar observation has been reported earlier [6]. Creep cavity was found to nucleate at the weld interface (Fig. 6(a)) and the cavitation was associated with coarse particles at the weld interface (Fig. 6(b)).

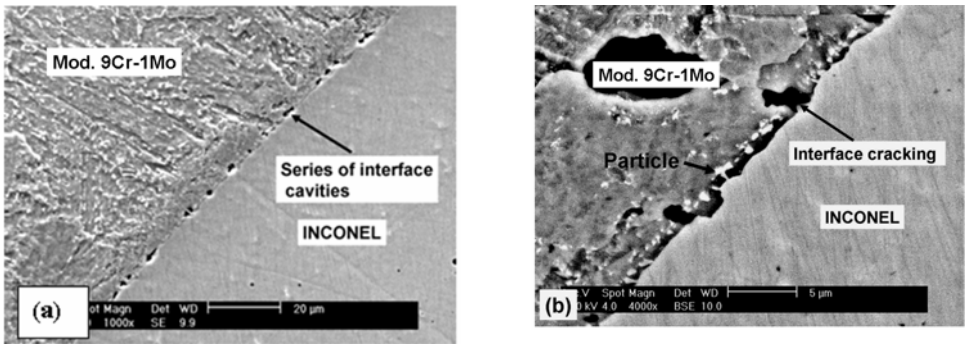

Fig. 6: (a) - Series of creep cavities at the weld interface; (b) - Cavities are associated with interface particles of in Mod. 9Cr-1Mo dissimilar weld joint creep tested at 180 MPa (t_r = 7503).

FE Analysis of Stress Distribution Across the Joint

The variation of creep deformation resistance of the different constituents of the weld joint as a function of applied stress at 823 K is shown in Fig. 7. Intercritical HAZ had the lowest creep deformation strength and the Inconel weld metal had the highest creep strength among the constituents of the joints. The steady state creep rate variation with applied stress obeyed a power law relation as $\dot{\varepsilon}_s = A\sigma^n$. Table 2 shows the values of the constant A and n of the various constituents of the joint, which were used in FE analysis as constitutive material model.

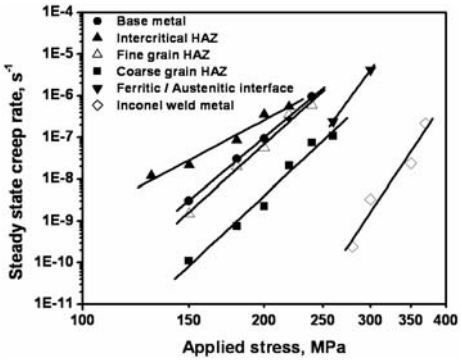

Fig. 7: Variation of steady state creep rate with stress of the different constituents of Mod. 9Cr-1Mo weld joint.

Table 2: Values of the constant n and A in creep rate equation $\dot{\varepsilon}_s = A\sigma^n$ for different microstructural constituents of Mod. 9Cr-1Mo steel dissimilar weld joint.

Material	A	n
Mod. 9Cr-1Mo Base metal	3.6×10^{-39}	12.9
Mod. 9Cr-1Mo ICHAZ	1.5×10^{-31}	10.1
Mod. 9Cr-1Mo FGHAZ	6.9×10^{-41}	13.7
Mod. 9Cr-1Mo CGHAZ	4.4×10^{-47}	15.6
Ferritic/austenitic weld interface	3.3×10^{-33}	10.9
Inconel Weld Metal	3.2×10^{-63}	21.7

Difference in creep deformation characteristics of the constituents of weld joint leads to stress redistribution across it [18]. Further, the constraint-creep deformation results in multiaxial state of stress across the weld joint, as in the case of notch specimens, thus influences the creep deformation and rupture behaviour of the weld joint. Finite element analysis of stress distribution across the weld joint revealed that the stress distribution across the dissimilar weld joint varies with creep exposure until it approaches to a stationary state, as shown in Fig. 8. In the weld joint, the near centre region was expected to deform in plane strain condition because of the constraint effect by the surrounding material, whereas, the near surface region under plane stress conditions because of the relatively unconstraint free surface.

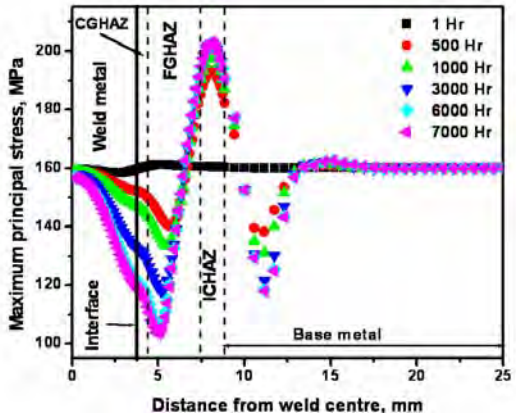

Fig. 8: Variation of estimated principal stress across the weld joint at the centre line location of it with creep exposure, creep tested at 160 MPa and 823 K.

Creep cavity nucleation is generally associated with the stress concentration at the discontinuities like precipitate, ledges, grain boundary triple points etc. If the stress concentrations, produced when deformation is held up by a finite amount of material around discontinuity like precipitate, are not relaxed, then cavities nucleate at the precipitate/matrix interface by athermal decohesion of atomic bonds between the precipitate and matrix [23]. Earlier studies have shown that von- Mises stress and maximum principal stress determines the cavitation behaviour of the materials [24]. As the shear stresses are associated with the von- Mises stress, this stress plays a significant role for the cavitation its magnitude reflects the extent of cavity nucleation. Fig. 9 shows the distribution of the von- Mises stress across the weld joint. The von- Mises stress was found to be maximum near surface of ferritic/austenitic weld interface than other regions of weld joint, indicating the possibility of creep cavity nucleation at the near surface region of ferritic/austenitic weld interface.

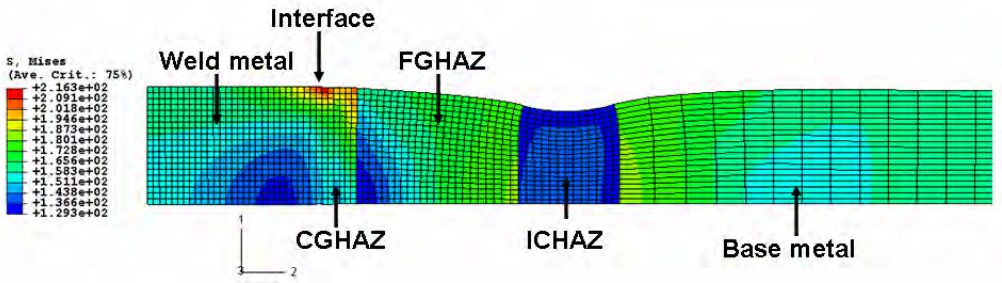

Fig. 9: Distribution of estimated von- Mises stress across the weld joint 7000 hours of creep exposure at 160 MPa and 823 K.

Though nucleation of creep cavities are expected to depend on von- Mises stress, their stability and subsequent growth is determined by the following expression:

$$r_c = 2\gamma_c / \sigma_1$$

where, r_c is the critical size of cavity, γ_c is the surface energy and σ_1 is the maximum principal stress. For the growth of existing cavity, it has to attain the critical size otherwise the cavity will sinter. As the principal stress was found to be higher in near surface region of ferritic/austenitic weld interface than other constituents of the weld joint, (Fig. 10), the cavity would reach critical size earlier in this region than in other zones of the weld joint and facilitate the growth leading to cracking and final fracture.

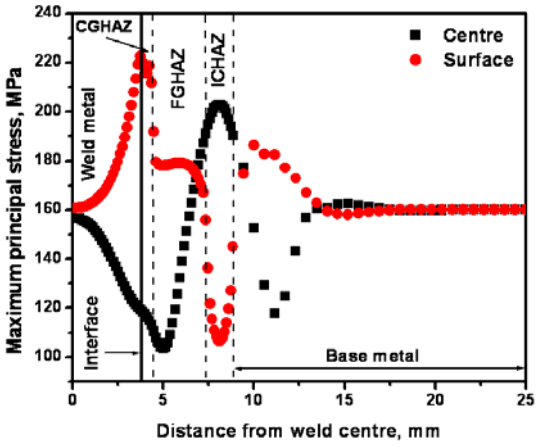

Fig. 10

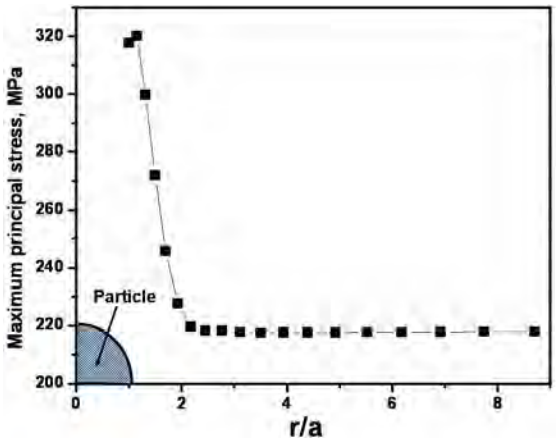

Fig. 11

Fig. 10: Variation of estimated principal stress across the weld joint at centre and near surface region after 7000 hours of creep exposure at 160 MPa and 823 K.

Fig. 11: Variation of estimated maximum principal stress in ferritic/austenitic weld interface around precipitate along the loading line.

Weld interface cracking in dissimilar weld joint was found to be associated with nucleation of creep cavities at the precipitate, Fig. 6. The precipitate particle embedded in matrix disturbs both the stress and strain fields around it [25].

Stress distribution around a spherical particle of 0.2 μm radius embedded in ferritic/austenitic weld interface was estimated by FE analysis considering the maximum stress (218 MPa) developed at near surface region of ferritic/austenitic weld interface due to strength inhomogeneity across the joint, creep exposed at 160 MPa and 823 K (Fig. 8). Fig. 11 shows the variation of principal stress along the loading line at 218 MPa and 823 K for 7000 hours of creep exposure.

In this figure, r represents the field point distance from the centre of the spherical precipitate and a is the radius of the spherical precipitate. The maximum principal stress was found to be maximum in the matrix near the particle/matrix interface and reduced to the far field values beyond a distance around three times of particle radius from the interface. This indicates that though the stresses in far field region would be equivalent to the applied stress but the strength homogeneity and existence of precipitates increases the level of stresses twice of the applied stress.

CONCLUSIONS

Based on the studies of creep behaviour of modified 9Cr-1Mo steel / Alloy 800 dissimilar joint and finite element analysis of stress distribution across the joint and precipitate particles, following conclusions have been drawn.

1. Dissimilar weld joint of ferritic and austenitic steel possessed lower creep rupture strength than the ferritic steel base metals.
2. At lower stress the failure in dissimilar weld joint occurred in the ferritic-austenitic weld interface.
3. Weld interface failure was associated with the creep cavitation at the interface particles under higher stress concentration resulting from higher creep strength gradient across the interface.
4. High maximum principal stress and von- Mises stress at near surface region of ferritic-austenitic weld interface and around the precipitate particle facilitate creep cavity nucleation and growth in this region.

ACKNOWLEDGEMENTS

The authors express their deep sense of gratitude to Mr. S. C. Chetal, Director, Indira Gandhi Centre for Atomic Research (IGCAR), Kalpakkam and Dr. T. Jayakumar, Director, Metallurgy and Materials Group, IGCAR for their keen interest in this work and encouragement.

REFERENCES

[1] Bhaduri, A.K., Venkadesan, S., Rodriguez, P., and Mukunda, P.G., "Transition metal joints for steam generators- An overview" *Int. J. Pres. Ves. Piping*, Vol. 58, 1994, pp. 251-265.

[2] Parker, J.D., "High temperature failure of thick-section, low alloy steel to stainless steel transition welds", *Mater. High. Temp.*, Vol. 12, 1994, pp. 25- 33.

[3] Parker, J.D., and Stratford, G.C., "Characterization of microstructures in nickel based transition joints", *J. Mater. Sci.*, Vol. 35, 2000, pp. 4099- 4107.

[4] Gong, Y., Cao, J., Li-na, J., Yang, C., Yao, C., Yang, Z.G., Wang, J., Luo, X.M., Gu, F.M., Qi, A.F., Ye, S.Y., Hu, Z.F., "Assessment of creep rupture properties for dissimilar steels welded joints between T92 and HR3C", *Fatigue Fract. Engng. Mater. Struct.*, Vol. 34, 2011, pp. 83- 96.

[5] Laha, K., Chandravathi, K.S., Bhanu Sankara Rao, K., Mannan, S.L., and Sastry D.H., "An assessment of creep deformation and fracture behaviour of 2.25Cr-1Mo similar and dissimilar weld joints", *Met. and Mats. Trans. A*, Vol. 32, 2001, pp.115-124.

[6] Yamazaki, M., Watanabe, T., Hongo, H., and Tabuchi, M., "Creep rupture properties of welded joints of heat resistant steels", *J. Power and Energy Systems*, Vol. 2, 2008, pp.1140-1149.

[7] An, J., Jing, H., Xiao, G., Zhao, L., and Xu, L., "Analysis of the creep behavior of P92 steel Welded Joint", *J. Mat. Eng. Perfor.*; 06 November 2010, online.

[8] Gauzzi, F., and Missori, S., "Microstructural transformations in austenitic-ferritic transition joints", *J. Mat. Sci.*, Vol. 23, 1988 pp. 782-789.

[9] Klueh, R.L., and King, J.F., "Austenitic stainless steel-ferritic steel weld joint failures", *Welding Journal*, Vol. 61, 1982, pp. 302–311.

[10] Roberts, D.I., Ryder, R.H., and Viswanathan, R., "Performance of dissimilar welds in service", *ASME Trans. J. Pres. Ves. Technol*., Vol. 107, 1985, pp. 247-254.
[11] Dehmolaei, R., Shamanian, M., and Kermanpur, A., "Microstructural characterization of dissimilar welds between alloy 800 and HP heat-resistant steel", *Mater. Cheract*., Vol. 59, 2008, pp.1447-1454.
[12] Nelson, T.W., Lippold, J.C., and Mills, M.J., "Nature and evolution of the fusion boundary in ferritic-austenitic dissimilar metal welds - Part 2: On-Cooling Transformations", *Welding Journal*, *Res. Suppl.*, 2000, pp.267s-277s.
[13] McPherson, N.A., Baker, T.N., and Miller, D.W., "A study of the structure of dissimilar submerged arc welds", *Met. Mater. Trans*., Vol. 19, 1997, pp. 823-832.
[14] DuPont, J.N., and Kusko, C.S., "Martensite formation in austenitic/ferritic dissimilar alloy welds", *Welding Journal*, *Res. Suppl*., 2007, pp. 51s-54s.
[15] Evans, R.W., and Wilshire, B., "An analysis of the creep fracture characteristics of austenitic/ferritic steel transition welds", *Mech. Mater*., Vol. 4, 1985, pp. 51-65.
[16] Tu, S.T., Segle, P., and Gong, J.M., "Strength design and life assessment of welded structures subjected to high temperature creep", *Int. J. Pres. Ves. and Piping*, Vol. 66, 1996, pp.171-186.
[17] Besson, J., Madi, Y., Motarjemi, A., Kocak, M., Martin, G., and Hornet, P., "Crack nucleation and propagation close to the interface in a ferritic- austenitic joint", *Mater. Sci. Eng. A*, Vol. 397, 2005, pp. 84-91.
[18] Hall, F.R., and Hayhurst, D.R., "Continuum damage mechanics modeling of high temperature deformation and failure in a pipe weldment", *Proc. Roy. Soc. Lond. (A)*, Vol. 433, 1991, pp. 383-403.
[19] Hayhurst, D.R., Goodall, I.W., Hayhurst, R.J., and Dean, D.W., "Lifetime predictions for high temperature low alloy ferritic steel weldments", *J. Strain Analysis*, Vol. 40, 2005, pp. 675-701.
[20] Hyde, T.H., Sun, W., and Becker, A.A., "Failure prediction for multi material creep test specimens using a steady state creep rupture stress", *Int. J. Mech. Sci*., Vol. 42, 2000, pp. 401-423.
[21] Hyde, T.H., and Sun, W., "A method for estimating the stress distributions on the centre line of an axisymmetric, two material, cross weld, creep test specimen", *Int. J. Mech. Sci*., Vol. 39, 1997, pp. 885-898.
[22] Hayhurst, D.R., Dimmer, P.R., and Chernuka, M.W., "Estimates of the creep rupture lifetime of structures using the finite element method", *J. Mech. Phys. Solids*, Vol. 23, 1975, pp. 335- 355.
[23] Smith, E., and Barnby, J.T., "Nucleation of grain boundary cavities during high temperature creep", *Met. Sci. J*., Vol. 1, 1967, pp. 1-4.
[24] Cane B.J., and Middleton, C.J., "Intergranular creep cavity formation in low alloy bainitic steels", *Met. Sci. J*., Vol. 15, 1981, pp. 295-301.
[25] Li, D., and Shinozaki, K., "Simulation of role of precipitate in creep void occurrence in heat affected zone of high Cr ferritic heat resistant steels", *Sci. Tech. Welding Joining*, Vol. 10, 2005, pp. 544-549.